Contract No.:

This manuscript has been authored by Battelle Savannah River Alliance (BSRA), LLC under Contract No. 89303321CEM000080 with the U.S. Department of Energy (DOE) Office of Environmental Management (EM).

Disclaimer:

The United States Government retains and the publisher, by accepting this article for publication, acknowledges that the United States Government retains a non-exclusive, paid-up, irrevocable, worldwide license to publish or reproduce the published form of this work, or allow others to do so, for United States Government purposes.

Stable, High-Performing Bifunctional Electrodes for Anion Exchange Membrane-Based Unitized Regenerative Fuel Cells

Noor ul Hassan,[1] Prabhu Ganesan,[2] Aaron A. Lando,[3]

William E. Mustain[*,1] and Héctor R. Colón-Mercado*[*,3]*

[1]Department of Chemical Engineering, University of South Carolina, Columbia, SC 29208, USA

[2]Advanced Materials, Savannah River National Laboratory, Aiken, SC 29808, USA

[3]Advanced Manufacturing and Energy Sciences, Savannah River National Laboratory, Aiken, SC 29808, USA

*Corresponding authors: mustainw@mailbox.sc.edu; hector.colon-mercado@srnl.doe.gov

Keywords: Anion exchange membrane; regenerative fuel cell; bifunctional electrocatalyst; oxygen electrode; cyclic durability

Abstract

Anion exchange membrane unitized regenerative fuel cells (AEM-URFCs) are a promising technology for energy storage and electricity production; however, their efficiency is limited by the kinetics of the bifunctional oxygen electrode (BOE) where the oxygen evolution reaction (OER) and oxygen reduction reaction (ORR) occur. A particular concern when designing the BOE is that the OER and ORR have differing catalytic requirements, which make it challenging to develop effective bifunctional electrocatalysts with single active sites. In this study, we focus on advancing the BOE performance using Pt-IrO_x and Pt-$NiCoO_x$ electrocatalysts. Single-layer and dual-layer Pt-IrO_x BOEs were made, with the dual-layer electrode leading to improved performance due to efficient catalyst utilization in both modes. Using the dual-layer oxygen electrode paired with a PtRu/C hydrogen electrode, a round trip efficiency (RTE) as high as 50% (62 $\%_{iR\text{-}free}$) was achieved at 500 mA/cm^2 and operation for more than 24 hours, which included five one-hour-long H_2 generation and consumption cycles followed by one eight-hours-long cycle. To the best of our knowledge, this is the highest performance for AEM-URFCs reported to date. Lastly, the approach is extended to electrodes with a Pt loading of 0.5 mg/cm^2 and the IrO_x substituted by $NiCoO_x$.

Introduction

A unitized regenerative fuel cell (URFC) is a single device that can reversibly operate as both a fuel cell and an electrolyzer. A URFC can serve as an energy storage device (via water electrolysis) to store excess electricity in the form of hydrogen during peak production times. This is particularly attractive from intermittent renewable energy resources like solar, wind, tidal, etc. **(1 - 4)**, where a large amount of storage may be needed and traditional batteries would require a very large footprint. URFCs can also function as an energy conversion device (fuel cell mode) that generates electricity from the stored hydrogen and oxygen (either co-stored from electrolysis or from air). URFCs can be a high energy storage capacity, low cost, simple, compact, and environmentally friendly technology with advantages over conventional energy storage technologies **(5 - 10)**. Because of this, URFCs have received an increased amount of research attention in recent years.

Among existing URFC technologies, proton exchange membrane (PEM)-based systems have benefitted from the highest level of investment. As such, they are more mature and have shown the best round-trip efficiencies (RTE=$\frac{E_{FC}}{E_{EC}} x100$) to date – up to 60 % RTE **(11)** – as well as relatively good durability. Lim and Lee et al. **(12)** recently reported 51 % RTE using a Pt-Ir bifunctional electrocatalyst while operating at 400 mA/cm^2. Kus et al. **(13)** showed an RTE of 47 % at 400 mA/cm^2 and 31.8 % at 1.0 A/cm^2 utilizing a sandwich-like Pt-Ir bifunctional anode electrocatalyst. Similarly, Regmi et al., **(14)** reported 57 % and 60 % RTE at 1.0 A/cm^2 operating with air and O_2, respectively, at 80^o C. Peng et al., **(15)** demonstrated 53% RTE at 1.0 A/cm^2 with constant gas mode and continuously operated the system for 500 hrs with negligible performance degradation. Unfortunately, PEM-URFCs are expensive due to their acidic environment requiring

the use of specialized component materials (e.g. perfluorinated membranes) and platinum group metal (PGM)-based electrocatalysts.

Alternately, anion exchange membrane (AEM)-based technologies are emerging due to their less corrosive operating environment and possible use of low-cost membranes, inexpensive component materials, and PGM-free electrocatalysts while offering competitive performance. The operation of AEM-URFCs (Figure S1) is driven by the reactions at the hydrogen (Equation 1) and oxygen (Equation 2) electrodes, and the overall reaction (Equation 3).

$$4H_2O + 4e^- \leftrightarrow 2H_2 + 4OH^- \qquad E^o = -0.828V \qquad (1)$$

$$O_2 + 2H_2O + 4e^- \leftrightarrow 4OH^- \qquad E^o = 0.401V \qquad (2)$$

$$2H_2 + O_2 \leftrightarrow 2H_2O \qquad (3)$$

From a catalytic perspective, the lower potential required of the oxygen electrode in the AEM versus the PEM system decreases the number of oxygenated adlayers on the catalyst surface, lowering the catalyst-oxygen bond formation energy and thus reducing the overpotential of the ORR in alkaline compared to acid electrolyte **(16 - 17)** and making that electrode more active in alkaline than in acid **(18 - 19).** Additionally, the less corrosive alkaline environment allows for low-cost stack components (membranes, bipolar plates, air loop, cooling, etc.) to be used **(20)**. Fortunately, significant progress has been made recently in the development of oxygen electrocatalysts as well as stable and highly conductive AEMs and ionomers. These advances have led to increased device operational life in discrete fuel cells **(21 - 26)** and discrete electrolyzers **(27 - 31),** which has revived researchers' interest in AEM-URFCs.

Several AEM-URFC prototypes have been reported in the literature **(32 - 38)**; however, their performances and round-trip efficiencies (summarized in Table S1 in the Supporting Information file) are still lower than those of PEM-based URFCs. For instance, Ng et al., **(34)**

reported RTEs of 42-45% at 20 mA/cm^2 operating at 55^o C. Bretthaur et al., **(39)** reported 52 % RTE at a very low current density of 0.1 mA/cm^2 using lanthanum-based electrocatalyst materials. Such very low current densities are not suitable for practical applications. Gayan and Ramani et al., **(40)** recently touted an AEM-URFC using a Pt-pyrochlore bifunctional oxygen electrocatalyst that achieved a RTE of 75% at 100 mA/cm^2, but the RTE was only ~36% at a more commercially-relevant operating current of 500 mA/cm^2. The best performing AEM-URFC in the literature to date was recently reported by Yan and co-workers **(41)** where the RTE at 500 mA/cm^2 was 48%. They were also able to show one-hour cycling durability with ~ 10 mins each cycle.

From the above literature data, it is clear that AEM-URFCs have shown lower operating current densities and higher degradation rates than PEM-URFCs. This is true even with the PGM-based catalysts that have been carried over from PEM-URFCs. In these cells, combinations of Pt and IrOx have been used at the oxygen electrode – the need for both being in the oxygen electrode is driven by the fact that the ORR and OER require different active sites since their rate determining steps (RDS) and the electrocatalyst surfaces are completely different under ORR and OER conditions **(42-43)**. In PEM-URFCs, this has been mostly accommodated by mixing Pt and Ir, the most stable and mature catalysts for ORR and OER, together in one electrode. This allows them to be operated as a mixture of their base metals (in FC mode) and oxides (in electrolyzer mode) in traditional URFCs **(45 - 49)**. These bimetallic composites of Pt-Ir have been shown to efficiently enable both OER and ORR on the same electrode **(12 - 14)** in PEM-URFCs.

The mixing of Pt and Ir in the PEM-URFC electrode has been accomplished in a number of ways. Various combinations of Pt and Ir (or IrO_x) have been investigated where their elemental ratio, catalyst preparation method, microstructure, etc. have been manipulated. From a catalyst perspective, there does not seem to be a consensus in the literature for the optimal ratio between

Pt and Ir. In typical studies, the proportion of Ir (or IrO_x) can range from 1 wt% to 50 wt% as shown in Table S2. In general, it is believed that the proportion of Pt should be more than half of the total metal loading, due to the incapability of Ir towards the ORR. For instance, Jung et al., **(67)** investigated various ratios of Pt:Ir and found that 85:15 Pt:Ir (wt:wt) was the best, achieving a RTE of 49 % at 500 mA/cm^2. At the electrode level, the most commonly employed method of combining Pt and Ir is mechanical mixing as it is an easy and direct method for the preparation of a composite bifunctional oxygen electrode (BOE). However, it has been found that agglomeration tends to occur quickly after mixing, which hinders fine dispersion of different catalyst components. To solve this problem, different synthesis methods have been developed to replace direct mixing, including Pt supported on IrO_x, IrO_x deposited onto Pt, or the use of multi-layer electrodes where catalysts are separately deposited in discrete layers (Table S2). In general, better particle dispersion and less agglomeration has been achieved in multi-layer structures **(68)**. Unfortunately, the effects of electrode structure and the integration of OER and ORR catalysts in AEM-URFCs has not been studied well. It is important to find the right balance and configuration of these materials – thus increasing the dispersion of active sites – which can be done through catalyst and/or electrode design and optimization. Also desirable in AEM-URFCs is to transition away from PGM-containing catalysts in order to reduce the cost compared to PEM-URFCs.

Therefore, in this work, two approaches were taken. The initial approach was to create a Pt-IrO_x BOEs with multiple structures. Pt and IrO_x were chosen to first understand how composite electrodes behave in AEM-URFC systems and investigate whether the learnings from PEM-URFCs can be directly translated to AEM-URFCs. The first electrode structure was comprised of a single-layer electrode. The second electrode structure was comprised of two layers where an IrO_x base layer was first deposited onto the porous transport later (PTL) followed by a Pt top layer,

which was in direct contact with the AEM in the membrane electrode assembly (MEA). The idea behind the layered electrode configuration was to enhance the access to the active sites in each mode and boost the cell performance while maintaining the OER catalyst at a distance from the AEM. The performance and durability of these two electrode types are compared. Additionally, the ionomer content of the oxygen electrode was optimized and the inclusion of Nafion™ as a binder in the OER electrode was studied. The other approach in this work extended the dual-layer electrode concept to a low-PGM electrode where the IrO_x was substituted by $NiCoO_x$. The performance and cyclability of this configuration are demonstrated and discussed. The state-of-the-art AEM-URFC performance and cycling results summarized in Table S1 opens doors for further development of AEM-URFCs, including alternate PGM-free electrocatalysts that will allow researchers to realize the true promise of alkaline based devices.

Materials and Methods

Materials

Three catalysts, 75 wt% PtRu on high surface area advanced carbon support (Alfa Aesar 47371; Platinum, nominally 50%, Ruthenium nominally 25%), Pt black (HiSPEC™ 1000), and IrO_x (Premion®, 99.99% metal basis and Ir 84.5% min) were purchased from Alfa Aesar. 2-Propanol (ACS reagent >99.5%) and potassium hydroxide (BioXtra, >85% KOH basis) were purchased from Sigma-Aldrich®. Vulcan® XC-72R carbon black was obtained from Cabot Corporation. Nickel cobalt oxide (99% trace metal analysis basis, <150 nm particles) was obtained from Sigma-Aldrich®. Low molecular weight anion exchange resin (TM1 Durion™ from Orion Polymer), 5 wt% wet proofed Toray carbon paper (TGP-H-060), Pention™ Membranes (30 μm Pention-AEM-72-30-15% and 5 μm Pention-AEM-72-5-15%, both 15% crosslinked), and D520

Nafion^{TM} dispersion ionomer (alcohol based 1000 EW at 5wt%) were purchased from the Fuel Cell Store. All materials were used as received.

Ink preparation

URFC oxygen electrodes were prepared by spray coating carbon paper PTLs with Pt-IrO_x for the oxygen electrode and PtRu/C for the hydrogen electrode. Two electrode designs were considered for the oxygen electrode – a single-layer and a dual-layer configuration. The ink for the single-layer oxygen electrodes was prepared by mixing the appropriate amounts of TM1 resin with 2.4 mL of deionized water and 3.3 mL of 2-propanol and mixing the components ultrasonically for 90 minutes at 40 ºC. Once all of the resin was dispersed, if used, an appropriate amount of Nafion^{TM} dispersion was added into the solution and vortex mixed. After the solution cooled to room temperature, 125 mg of IrO_x and 62.5 mg of Pt black were added under a blanket of inert atmosphere. Once the catalyst was well incorporated, 20.7 mL of 2-propanol was added. The resulting slurry was then ultrasonically mixed for an additional 90 minutes in an ice bath. Specific amounts of anion exchange resin (TM1), Nafion^{TM} (D520) and the ionomer to catalyst ratio (I/C) are listed in Table 1. A similar catalyst ink preparation method was used for PGM-free/low-PGM catalysts.

Table 1. Electrode ink composition mixed with 125 mg of IrO_x and 62.5 mg Pt black in 2.4 mL of H_2O and 24 mL of 2-propanol. Note-I/C includes both TM1 and D520.

TM1/D520 Dry wt%	I/C	TM1 (mg)	D520 (µL)
15/0	0.178	33.0	0
15/2	0.206	34.0	100
15/4	0.234	34.7	200
20/0	0.251	47.0	0
20/2	0.283	48.2	105
20/4	0.321	50.0	220
25/0	0.336	63.0	0
25/2	0.370	64.0	115
25/4	0.407	66.0	225
35/2	0.589	104.5	129
35/4	0.640	107.6	267

To prepare the dual-layer oxygen electrodes, two inks were prepared, one containing IrO_x and the other containing Pt black. Similar solvent composition and polymer amounts were used as in the single-layer electrode. In the first ink, 43.5 mg of TM1 resin was mixed with 2.4 mL of deionized water and 3.3 mL of 2-propanol followed by ultrasonic mixing for 90 min. at 40 ºC. Once all of the resin was dispersed and after the solution was cooled to room temperature, 130.4 mg of IrO_x was added in an inert atmosphere followed by 20.7 mL of 2-propanol. The mixture was then sonicated for an additional 90 min. in an ice bath. In the second ink, the same recipe and procedure was employed except that 65.4 mg of Pt black and 21.8 mg of TM1 were used. The optimized I/C ratio was used to prepare low-PGM single- and dual-layer oxygen electrodes. The procedures and solvent mixtures previously described were followed, however $NiCoO_x$ was used instead of IrO_x as the OER catalyst.

The ink for the hydrogen electrodes was prepared by ultrasonically mixing 91 mg of TM1 resin with 3 mL of deionized water and 6 mL of 2-propanol for 90 minutes at 40 ºC. Once all of the resin was dispersed, 150 µL of Nafion™ D520 dispersion was added, and vortex mixed. After cooling to room temperature, 240 mg of PtRu/C and 120 mg of Vulcan® XC-72 were added under

an inert atmosphere. Once all the catalyst was fully incorporated into the slurry, 18 mL of 2-propanol was added to the mixture and ultrasonically mixed for an additional 90 min. in an ice bath.

Electrode Fabrication

All electrodes were fabricated using an automated ultrasonic sprayer (Prism-400BT, Ultrasonic Systems, Inc.). Initially, the ink was loaded into the system and mechanically mixed for an additional 30 minutes before spraying. Carbon paper PTLs (Toray 60 with 5% wetproofing) having 25 cm^2 area were placed on a heated vacuum plate (at 60 ºC) and coated with the desired catalyst loadings. While carbon is typically avoided for high voltage operation, commercially available wet proofed carbon paper PTLs are considered a low-cost and easily accessible alternative for short-term testing as opposed to more costly metal based PTLs that will require wet proofing optimization **(58)**. To ensure low/negligible carbon oxidation in our tests, the operating potentials and current density were maintained below 2 V and 1.0 A/cm^2 respectively **(59)**. The ink was sprayed at a flowrate of 500 µL/minute, a nozzle speed of 60 mm/s, and a nozzle height of 50 mm. The hydrogen electrode metal loading (Pt+Ru) was maintained at 1.25 ± 0.05 mg_{metal}/cm^2 and the total oxygen electrode loading (Pt+IrO_x) was kept at 2.6 ± 0.05 mg/cm^2 for single- and dual- layer electrodes. Dual-layer oxygen electrodes were prepared by first spraying the IrO_x ink (~1.6 mg_{IrOx}/cm^2) followed by the Pt black ink (~1.0 mg_{Pt}/cm^2). Low PGM single- and dual-layer oxygen electrodes were prepared following the procedures previously described. However, the electrodes were made with $NiCoO_x$ (1.10 or 2.00 mg/cm^2) and Pt black (0.50 mg/cm^2).

Cell assembly

Prior to the cell assembly, 5 cm^2 electrodes were cut from the larger 25 cm^2 electrodes. The cut electrodes and the membrane were then immersed in 1 M KOH solution. The solution was changed every twenty minutes three times to ensure full ion exchange and to minimize any carbonates. Immediately afterwards, the components were loaded into electrolyzer hardware (Scribner Associates, Inc.) with triple serpentine flow-fields. Glass reinforced silicone gaskets (165 μm) were used to control the degree of compression, resulting in a pinch of around 25%. Once the MEA was assembled, the bolts holding the cell hardware together were tightened with a torque of 3.4 N-m each.

URFC Testing

Short-term testing was performed using an Arbin Instruments fuel cell test station. During cell start up, humidified nitrogen was purged at a rate of 750 sccm to the anode and cathode until the cell reached the operating temperature of 60 ºC. The humidifiers were set to 58 ºC and 56 ºC for the oxygen and for the hydrogen side, respectively. Once all of the set temperatures were stable, the nitrogen flow was stopped and switched to oxygen (cathode) and hydrogen (anode) to operate the cell in fuel cell mode. To break the cell in, the cell was polarized to 0.5 V to activate the MEA for 5 minutes. Then, polarization curves were recorded from the open circuit voltage (OCV) to 0.1 V every five minutes until stable performance was obtained. Once steady polarization behavior was achieved, two fuel cell polarization curves were recorded and a reductive current density of 500 mA/cm^2 was applied for a desired duration. After the constant current run, the cell was allowed to rest back to the OCV, and the gases were switched to humidified nitrogen. To initiate the electrolyzer mode, a 0.1 M KOH was fed to the oxygen electrode at a rate of 0.3 mL/min. The

cell was allowed to equilibrate for 10 minutes prior to collecting a polarization curve from OCV to 2.0 V or 1.0 A/cm^2. After the polarization, an oxidative current of 0.5 A/cm^2 was applied for a desired time. To switch back to fuel cell mode, the liquid feed was stopped, and the gases were switched back to oxygen and hydrogen at 750 sccm. After keeping the cell at OCV for one minute, two fuel cell polarization curves were collected, and the cycle was repeated. After the second cycle, the high frequency resistance (ca. 10 kHz) was measured under open circuit conditions (10 mV amplitude) and 0.1 M KOH flow by means of potentiostatic electrochemical impedance spectroscopy using a potentiostat (HCP-803, Biologic).

Longer term cycling was performed using two separate test stations; a Scribner 850E was used for fuel cell testing while an Arbin BT2000 was used for electrolyzer testing. A similar procedure was applied for longer term cycling. First, in FC mode, nitrogen gas with full humidification was fed to both electrodes and the cell temperature was set to 60^o C. When the cell temperature was stabilized, hydrogen and oxygen were fed to respective electrodes and a break-in procedure was applied where the cell was gradually polarized from OCV to 0.1 V. Next, the hydrogen and oxygen reacting gas dew points were optimized, and polarization curves were collected. The cell was then operated at 0.5 A/cm^2 for the desired time. To switch to electrolyzer mode, nitrogen was fed to both sides of the cell, replacing hydrogen and oxygen. The cell was then disconnected from the Scribner test station and connected to the Arbin. Then, dilute KOH (0.1 M, 1.6 mL/min) solution was constantly circulated to the oxygen electrode only while the cell temperature was maintained at 60 ^{o}C. Next, polarization curves were collected, scanning from 0.0 – 1.0 A/cm^2. After polarization, a constant current of 0.5 A/cm^2 was applied for a desired duration. To switch back to fuel cell mode, the 0.1M KOH flow was stopped and connected with the fuel cell test station while not allowing the cell temperature to drop. Cell temperature and gas

humidification temperatures were set to desired levels and the cell was operated again at a constant current density of 0.5 A/cm^2 after the temperatures were equilibrated.

Results and discussion

URFCs with single-layer oxygen electrodes were assembled and tested to better understand how two electrode-level variables influence cell performance, reversibility, and durability. The first variable was the inclusion of the Nafion^{TM} D520 binder. Nafion^{TM} has been widely used in the literature as a binder in AEM-URFCs **(27, 50 - 52)** to reduce catalyst detachment, despite the fact that it does not contribute to the ionic conductivity of the electrode. In fact, Nafion^{TM} ionomers and the AEM polymer resin could be incompatible and differences in the thermal and hydrated expansion of the interface between the Nafion^{TM} ionic binder and catalyst could result in performance loss **(52)**. Moreover, it is possible that there is some charge neutralization at the AEM:PEM interface, which can reduce water mobility and OH^- transport. Figure 1 shows polarization and steady-state voltage response data for an electrode with only the TM1 anionomer and an electrode with both TM1 and Nafion^{TM} D520. In Figure 1a, the electrode employing only TM1 (I/C=0.336) showed very good performance in both fuel cell and electrolyzer modes. At the target operating current density of 500 mA/cm^2, the TM1 electrode was able to operate at a cell voltage of 1.49 V as an electrolyzer and 0.77 V as a fuel cell, resulting in a round-trip-efficiency of 52 %. At 1.0 A/cm^2, this configuration also performed well, with the ability to achieve an electrolyzer voltage of 1.57 V, fuel cell operating voltage of 0.69 V and round-trip efficiency of 44 %. Increased amounts of TM1 and Nafion^{TM} D520 markedly reduced the performance and the cell voltages in both modes were negatively impacted. At 500 mA/cm^2, the electrolyzer operating voltage increased to 1.62 V, while the fuel cell voltage was reduced to 0.69 V, which resulted in a

compromised RTE of 43 %. Additionally, the polarization curves in both modes showed a lower achievable current, and a clear transition to mass-transport controlled conditions, most likely due to reduced water and anion transport. The negative effect of Nafion^{TM} D520 and excess TM1 addition was confirmed at steady-state as well, Figure 1b, where the operating voltages were worsened once Nafion^{TM} was added, and the voltage stability was reduced. These results show that although adding Nafion^{TM} ionomer can help catalyst adhesion, it reduces the overall URFC performance, suggesting that other strategies are needed to improve catalyst adhesion while employing anion-conducting materials in AEM-URFCs. Therefore, Nafion^{TM} was not used in any other electrodes in this study.

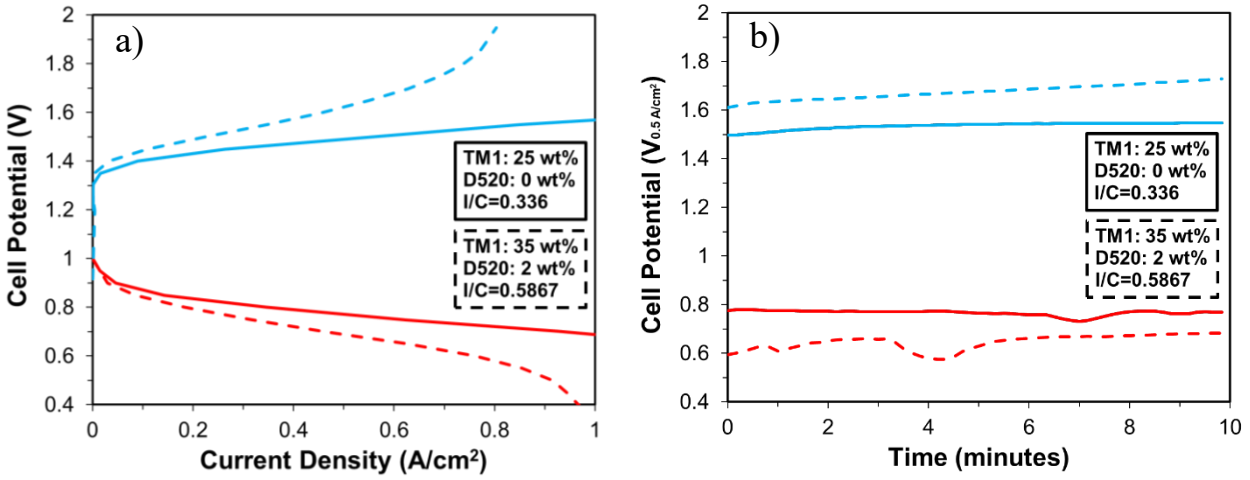

Figure 1. URFC performance for electrodes prepared with 25 wt% TM1 (I/C-0.336, solid lines) and with 35 wt% TM1 + 2 wt% D520 (I/C=0.587, dashed lines). a) URFC polarization curve and b) potential response as a function of time under a current hold of 0.5 A/cm^2. Hydrogen electrode: 1.27 mg/cm^2 PtRu/C, 750 sccm H_2 or N_2, 1 bara; Oxygen electrode: 2.6 mg/cm^2 Pt+IrO_x, 750 sccm O_2 or 0.3 mL/min 0.1 M KOH; Membrane: Pention-AEM-72-30-15%; Cell size: 5 cm^2.

The second variable that was investigated in the single-layer electrodes was the ionomer/catalyst (I/C) ratio. Oxygen electrodes with several I/C ratios listed in Table 1 were prepared and tested. Both polarization and steady-state measurements were made. The results of

10 minute cycle (2nd cycle, iR-free) steady-state voltage measurements at 500 mA/cm^2 are shown in Figure 2. The results show a mostly flat fuel cell response, though the electrolyzer performance shows a gradual decrease in electrolysis potential and a corresponding improvement in RTE up to an increase in the I/C ratio of 0.3-0.4. Beyond this ratio, an increase in cell voltage and decrease in RTE was observed. The data suggests that an I/C ratio in the range of 0.3-0.4 was optimal. At I/C=0.336, an RTE as high as 50% (62% based on iR-free cell voltage at 500 mA/cm^2) was obtained, which is one of the highest ever reported efficiency values in the literature for PEM or AEM URFCs **(15)**. The optimum I/C ratio of 0.3-0.4 yields an approximate ionomer content of 25 wt% (I/C=0.336), which was used for the rest of the electrodes tested in this study.

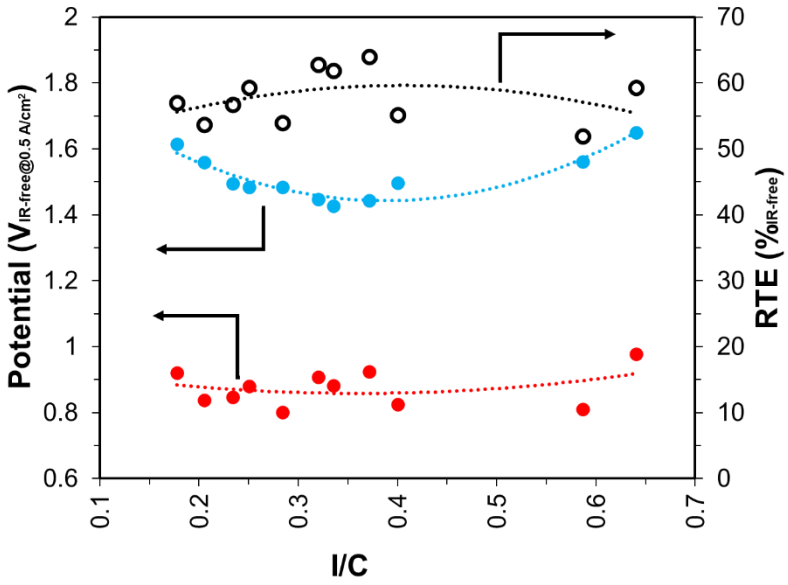

Figure 2. iR-free potential response at 0.5 A/cm^2 for the second cycle of electrodes evaluated for fuel cell (red line) and electrolysis (blue line) performance. Secondary y-axis shows the iR-free second cycle RTE (black line). Hydrogen electrode: 1.27 mg/cm^2 PtRu/C, 750 sccm H_2 or N_2, 1 bara; Oxygen electrode: ~2.6 mg/cm^2 Pt+IrO_x, 750 sccm O_2 or 0.3 mL/min 0.1 M KOH; Membrane: Pention-AEM-72-30-15%; Cell size: 5 cm^2.

Next, the cycling durability of an AEM-URFC with the optimized I/C ratio was investigated. Figure 3a shows polarization curves for optimized single-layer electrodes at the beginning of life (BOL). After collecting the BOL data, the cell durability was evaluated and is

reported in Figure 3b. During the durability experiment, the cell was tested cyclically in electrolyzer and fuel cell modes for one hour duration at each mode, while operating at a constant current density of 500 mA/cm^2. In electrolysis mode, the cell voltage was 1.58 V in the first cycle and increased to 1.62 V and 1.77 V at the end of 2nd and 3rd cycles, respectively. While operating in FC mode, the cell potential was 0.804 V during the first cycle and decreased to 0.774 V and 0.723 V at the end of 2nd and 3rd cycles, respectively. The corresponding RTE during cycling of the cell was ~ 50 % during the first cycle which then decreased to ~ 48% and ~ 46% for the 2nd and 3rd cycles, respectively. One of the reasons for the reduced performance with cycling was a gradual increase in area specific resistance (ASR) in just three cycles, where the measured ASR was 33 mΩ cm^2 at the beginning of the first cycle and increased to 67 mΩ cm^2 at the end of 3rd cycle. This accounts for ~ 17 mV degradation at 500 mA/cm^2, which was only a small fraction of the overall voltage change. Additional performance degradation during URFC operation can be due to catalyst detachment, though this was not observed in the present study. Another possible cause for reduced cell performance is reactant limitations at higher current densities due to a change in the wetting properties of the catalyst layer. Having both reactions occurring in a single-Pt-IrO_x catalyst layer can lead to degradation due to exposure of the ORR catalyst and ionomer to the OER reaction products and operating conditions, especially at high potentials, and vice versa. This can lead to diffusional limitations such as bubble trapping and electrode attrition due to gas evolution.

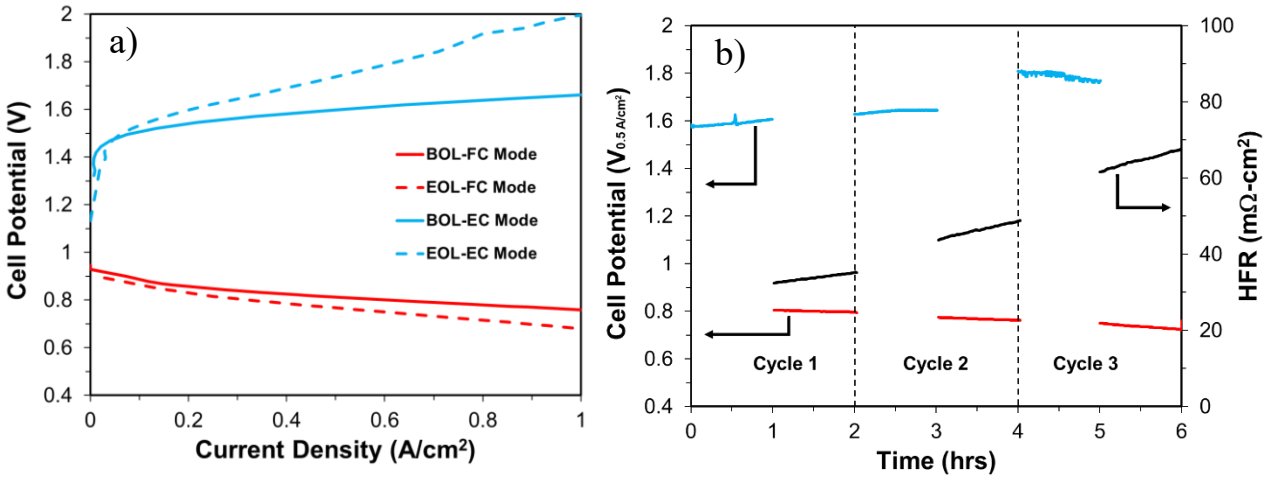

Figure 3 Single-layer electrode results: a) URFC polarization curve, the electrodes prepared with 25 wt% TM1 (I/C-0.336) BOL – solid lines and EOL – dashed lines. Hydrogen electrode: 1.27 mg/cm^2 PtRu/C, 1000 sccm H_2 or N_2, 1 bara; Oxygen electrode: 2.6 mg/cm^2 Pt+IrO_x, 1000 sccm O_2 or 1.6 mL/min 0.1 M KOH; Membrane: Pention-AEM-72-5-15%; Cell size: 5 cm^2. b) Potential response as a function of time under a current hold of 0.5 A/cm^2 – FC-red and EC-blue solid lines and HFR over time – black solid lines.

Therefore, an electrode design was conceived that would allow for each catalyst in the oxygen electrode to operate independently by creating a dual-layer oxygen electrode. In this configuration, an IrO_x layer was first deposited onto the PTL and then a Pt black layer was deposited on top of that as described in Materials and Methods section. Once assembled in a cell, the Pt layer is in intimate contact with the AEM, which is desired in FC mode where ionic mobility is only facilitated by the solid electrolyte. In electrolysis mode, an alkaline electrolyte (0.1 M KOH) is fed, which allows for ion transport in the liquid and solid phases from the outer layer to the AEM. In electrolysis mode, water and evolved oxygen are not required to rapidly penetrate the entire thickness of the catalyst layer as only the outer layer is electroactive.

The BOL and EOL polarization curves and cyclic durability of a dual layer MEA in an AEM-URFC are shown in Figure 4. As shown in Figure 4a, the BOL and EOL polarization curves were very similar. In fact, at the EOL, there was no change in overpotentials in the electrolysis mode while a slight decrease in voltage is recorded in FC mode due to an increase in the ASR at

the EOL. The cycling durability of the dual-layer electrode was also superior to the single-layer electrode, as shown in Figure 4b.

Starting with electrolysis mode, the cell voltage was 1.60 V during first cycle which remained unchanged after 5 cycles. In FC mode, the cell potential was 0.788 V (slightly lower than the single layer) during the first cycle and decreased to 0.754 V at the end of the 5^{th} cycle, which is an improvement of ~ 30 mV over the 3^{rd} cycle of the single-layer electrode. There was no significant increase in the ASR (increased from 51.5 $m\Omega.cm^2$ to 57 $m\Omega.cm^2$) during the first 5 cycles. The RTE was ~ 49.4 % at the start of cycle 1 and declined to ~ 48% at the end of 5^{th} cycle. For the 6^{th} cycle, the cell was exposed to one long-duration cycle of ~ 8 hrs in each mode, yielding a total continuous operating time of 26 hours. To the best of our knowledge, the present work shows the highest combination of RTE and cyclic durability at 500 mA/cm^2 for an AEM-URFC. However, improvements are still needed, and our future work will focus on further improving the performance and durability. The slight increase in ASR suggests that there is still a water deficiency when operating the URFC in fuel cell mode that needs to be addressed. It is also possible that some of the voltage decay can be related to the oxidation of carbon PTL in the oxygen electrode while operating at higher potentials for extended duration **(53)**.

Similar two-layer configurations have been studied in the literature for PEM-URFCs (Table S2). For example, Chen et al. **(69)** deposited a Pt layer directly onto the GDL and the Ir layer onto the membrane in a PEM-URFC. They concluded that the dual-layer approach showed a more homogeneous and porous surface than a single-layer electrode, which prevented water flooding at high current density in fuel cell mode. The current work shows a different configuration where the OER catalyst was first deposited onto the PTL followed by the ORR catalyst in such a way that the Pt black is in close contact with the AEM. Though slightly different

in conformation, the results indicate that the dual-layer electrodes are effective in AEM-URFCs, which, to the best of our knowledge, has not been reported previously.

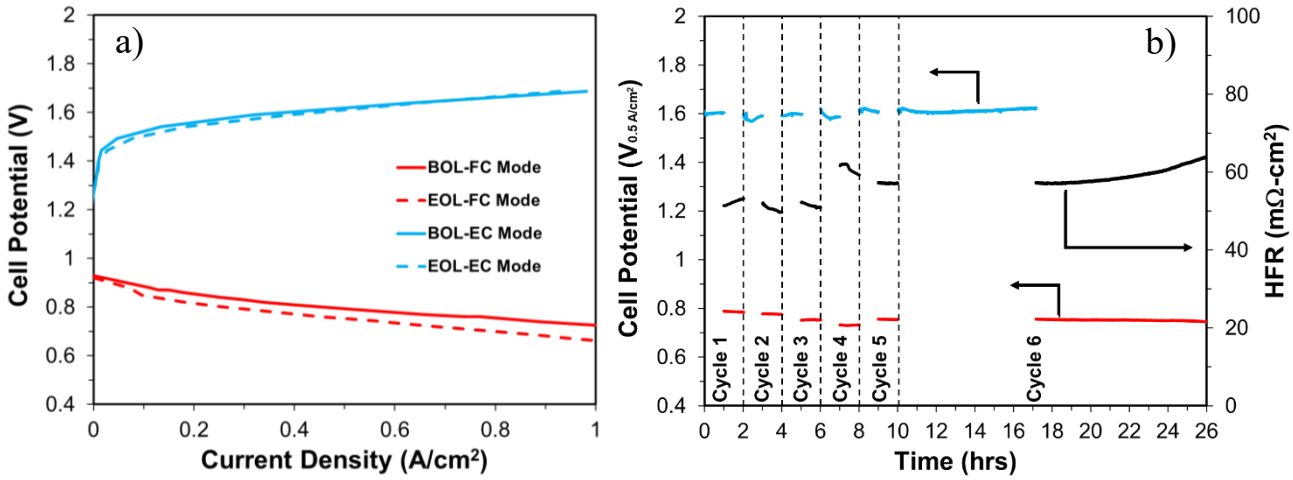

Figure 4. Dual-layer electrode results: a) URFC polarization curve, the electrodes prepared with 25 wt% TM1 (I/C-0.336) BOL – solid lines and EOL – dashed lines. Hydrogen electrode: 1.27 mg/cm^2 PtRu/C, 1000 sccm H_2 or N_2, 1 bara; Oxygen electrode: 2.6 mg/cm^2 Pt+IrO_x, 1000 sccm O_2 or 1.6 mL/min 0.1 M KOH; Membrane: Pention-AEM-72-5-15%; Cell size: 5 cm^2. b) Potential response as a function of time under a current hold of 500 mA/cm^2 – FC-red and EC-blue solid lines and HFR over time – black solid lines.

Another important focus for future work is the replacement of PGM-based catalysts with low-cost PGM-free metal catalysts. The use of low-cost cell construction materials and PGM-free electrocatalysts is one of the most often cited advantages of alkaline electrochemical systems and most of the studies in the literature continue to focus solely on PGM-containing materials. An important fact is that the stability of both ORR and OER catalysts over the entire potential window of operation (0.6-1.8 V) must be considered while designing a URFC BOE. Moreover, transition metal oxide PGM-free OER catalysts have been the focus of many recent studies **(60 - 64)**, showing relatively good performance and stability. The best-performing PGM-free ORR catalysts are mostly based on Fe-N-C type and despite their good ORR catalytic activity, these catalysts do not show good stability **(65, 66)**, especially at high potentials. Because of this, low PGM-loading oxygen electrodes were made that use Pt black as the ORR catalyst and commercial $NiCoO_x$ as

the OER catalysts to replace the expensive IrO_x. Also, the loading of Pt black was reduced to 0.5 mg/cm^2 resulting in PGM loading reduction from 2.6 mg/cm^2 to 0.5 mg/cm^2 or an 80% PGM catalyst reduction at the oxygen electrode. Figure 5 compares the effect of dual-layer and single-layer electrodes containing PGM-free OER catalyst. As observed in high PGM loading dual-layer electrodes, the low PGM loading dual-layer electrode showed superior performance compared to the single-layer electrode. These results support the notion that electrode structure and optimization can yield improvements in AEM-URFC performance and can be used to offset the lower performance normally observed with PGM-free catalysts.

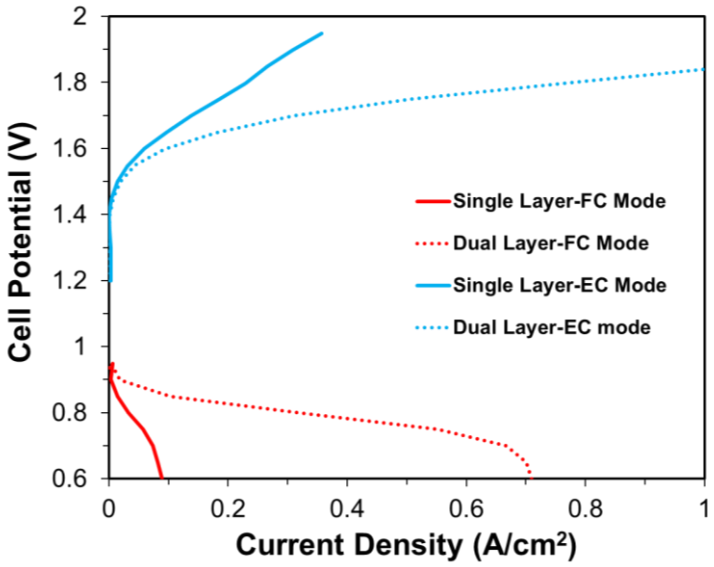

Figure 5. URFC polarization curves for low PGM single layer and dual layer bifunctional electrodes prepared with $NiCoO_x$ OER catalyst and low loading Pt black ORR catalyst at the oxygen electrode. Oxygen electrodes prepared with 25 wt% TM1 (I/C-0.336); Single layer – solid lines and Dual layer – dotted lines, FC-red and EC-blue solid lines. Hydrogen electrode: 1.27 mg/cm^2 PtRu/C, 750 sccm H_2 or N_2, 1 bara; Oxygen electrode: 1.1 mg/cm^2 $NiCoO_x$ and 0.5 mg/cm^2 Pt black, 750 sccm O_2 or 0.3 mL/min 0.1 M KOH; Membrane: Pention-AEM-72-5-15%; Cell size: 5 cm^2.

Next, the dual layer Pt-$NiCoO_x$ oxygen electrode was tested for its cycling durability. The BOL and EOL polarization curves and cyclic durability of a dual-layer MEA in AEM-URFC are shown in Figure 6. It is important to note that while the Pt loading is kept the same at 0.5 mg/cm^2, the $NiCoO_x$ loading was increased from 1.1 mg/cm^2 to 2.0 mg/cm^2. The increase in the OER

catalyst loading resulted in an increased electrolysis performance while improving the fuel cell performance. The increase in fuel cell performance can be explained as follows: the $NiCoO_x$ catalyst layer forms a microporous layer-like surface which facilitates uniform Pt deposition and increases Pt utilization for the ORR. With the increase in FC performance, the low PGM loading electrode performed as good as the single-layer or dual-layer high PGM-loading electrodes. As shown in Figure 6a, performance degradation is observed from BOL to EOL polarizations in both EC and the FC modes. For the EC mode, the electrode went through an initial catalyst deactivation period during the first 45 minutes of electrolysis operation (Figure 6b). After this deactivation region, the OER performance was stable during the test showing minimal degradation after 3 cycles (ca. 6 hrs of testing). On the other hand, no drastic voltage loss is observed in the FC mode; however, it did undergo a slow linear decay throughout the test.

Starting with operation in FC mode, the cell voltage was 0.789 V which is almost identical to that of the high PGM loading electrodes discussed in Figure 4. By the end of the third fuel cell cycle, the voltage decreased to 0.735 V (loss of 54 mV). This decrease was much higher than that observed in Figure 4 after 26 hrs of operation; however, the degradation was lower than the 80 mV of degradation observed after three cycles for the high PGM loading single layer electrode shown in Figure 3. In EC mode, the initial potential was 1.648 V at 0.5 A/cm^2 and after the initial deactivation in the first cycle, the voltage was 1.782 V. At the end of the third EC cycle, the voltage was 1.798 V. Disregarding the initial degradation step, only a 16 mV loss is observed for the PGM-free OER electrode which is significantly lower than the degradation by 192 mV observed in Figure 3 for the high PGM loading single-layer electrode. The RTE was 48 % prior to initial degradation. After the initial degradation, a RTE of 44% was obtained. At the end of the third cycle the final RTE was 41%. Apart from the previously discussed possible degradation

mechanisms, it is possible that the PGM-free OER catalyst degradation is affecting the ORR, though this is an area that is not well understood and is outside the scope of the present work. Certainly, this work shows complete replacement of the OER catalyst with a low-cost PGM-free material that is still able to operate at commercially relevant current densities (500 mA/cm^2) while achieving high RTE for an AEM-URFC.

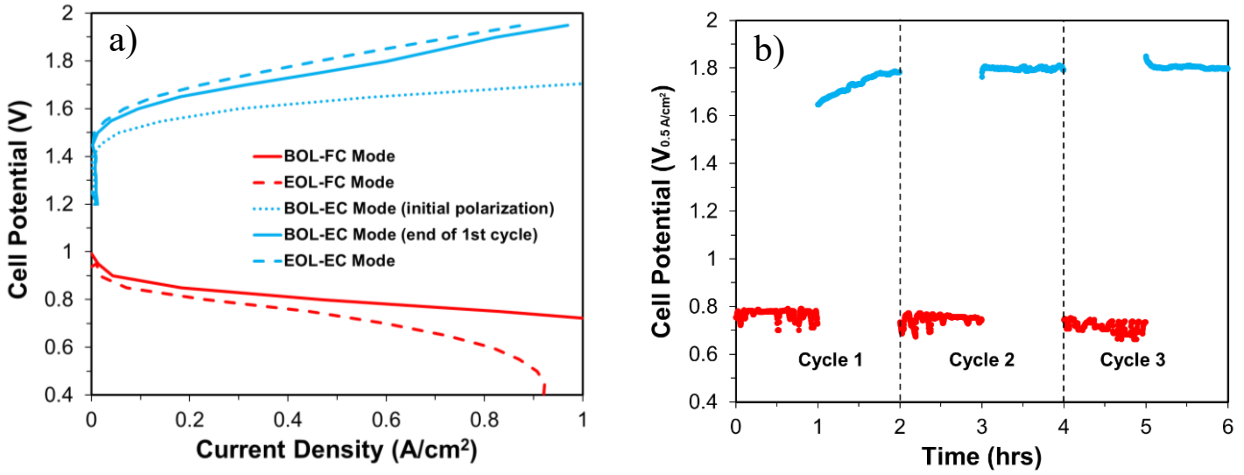

Figure 6. Dual-layer electrode results for a low PGM bifunctional oxygen electrode: a) URFC polarization curve, the electrodes prepared with 25 wt% TM1 (I/C-0.336) BOL – solid lines and EOL – dashed lines. Hydrogen electrode: 1.27 mg/cm^2 PtRu/C, 750 sccm H_2 or N_2, 1 bara; Oxygen electrode: 2.0 mg/cm^2 $NiCoO_x$ + 0.5 mg/cm^2 Pt black, 750 sccm O_2 or 0.3 mL/min 0.1 M KOH; Membrane: Pention-AEM-72-5-15%; Cell size: 5 cm^2. b) Potential response as a function of time under a current hold of 500 mA/cm^2 – FC-red and EC-blue solid lines.

Conclusions

In this study, the oxygen electrode for an AEM-URFC was studied with several configurations and catalyst layer compositions. The addition of Nafion^{TM} as a binder was evaluated as part of the electrode design and shown to increase catalyst layer adhesion, however, it had a negative effect on performance and durability due to an increase in Ohmic resistance. An ionomer to catalyst ratio of 0.336 was found to be optimal. Single-layer and dual-layer Pt-IrO_x BOE structures were prepared and tested in AEM-URFC. It was found that the dual-layer electrode structure resulted in an improved URFC performance due to efficient catalyst utilization

in both modes. The dual-layer electrode configuration, with an IrO_x layer deposited directly onto the PTL and a Pt layer deposited on the surface facing the AEM, resulted in higher URFC performance than a single-layer electrode. This structure also allowed for a significant improvement in long-term operation and electrode durability. The advances here resulted in AEM-URFC RTE of 50% and the successful completion of multiple 1-hour and an 8 hour cycle. Lastly, the dual-layer electrode structure was extended to low PGM loading BOE electrodes having 0.5 mg/cm^2 Pt for the ORR and up to 2.0 mg/cm^2 $NiCoO_x$ for the OER. The low PGM loading BOE showed comparable overall URFC performance to that of high PGM loading single- or dual-layer BOE. The low PGM loading BOE employing inexpensive $NiCoO_x$ exhibited an initial RTE of 48% and 7% reduction after a short-term durability cycling. These promising results obtained using dual-layer low PGM loading BOE opens new avenues for further optimization of inexpensive PGM-free electrocatalysts for AEM-URFC application.

Acknowledgments

This work was supported by the Laboratory Directed Research and Development (LDRD) program within the Savannah River National Laboratory (SRNL). This work was produced by Battelle Savannah River Alliance, LLC under Contract No. 89303321CEM000080 with the U.S. Department of Energy. Publisher acknowledges the U.S. Government license to provide public access under the DOE Public Access Plan (http://energy.gov/downloads/doe-public-access-plan).

References

(1) Bard, A. J; Fox, M.A. Artificial photosynthesis: Solar splitting of water to hydrogen and oxygen water splitting, *Acc. Chem. Res*. **1995**, 28, 141–145.

(2) Nocera, D.G; Nash, M.P. Powering the Planet: Chemical Challenges in Solar Energy Utilization, *Proceedings of the National Academy of Sciences of the United States of America*, **2006**, 103, 15729-15735.
(3) Nocera, D.G. Chemistry of personalized solar energy, *Inorg. Chem*, **2009**, 48, 10001–10017.
(4) Zhao, S; Yan, L; Luo, H; Mustain, W; Xu, H. Recent progress and perspectives of bifunctional oxygen reduction/evolution catalyst development for regenerative anion exchange membrane fuel cells, *Nano Energy*, **2018**, 47, 172–198.
(5) Wang, Y; Leung, D.Y.C; Xuan, J; Wang, H. A review on unitized regenerative fuel cell technologies, part B: Unitized regenerative alkaline fuel cell, solid oxide fuel cell, and microfluidic fuel cell, *Renew. Sustain. Energy Rev*. **2017**, 75, 775–795.
(6) Gabbasa, M; Sopian, K; Fudholi, A; Asim, N. A review of unitized regenerative fuel cell stack: Material, design and research achievements, *Int. J. Hydrogen Energy.* **2014**, 39, 17765–17778.
(7) Sadhasivam, T; Dhanabalan, K; Roh, S.H; Kim, T.H; Park, K.W; Jung, S. A comprehensive review on unitized regenerative fuel cells: Crucial challenges and developments, *Int. J. Hydrogen Energy,* **2017**, 42, 4415–4433.
(8) Kanan, M.W; Nocera, D.G. In situ formation of an oxygen-evolving catalyst in neutral water containing phosphate and Co2+, *Science*, **2008**, 321, 1072–1075.
(9) Gorlin, Y; Jaramillo, T.F. A bifunctional nonprecious metal catalyst for oxygen reduction and water oxidation, *J. Am. Chem. Soc.* **2010**, 132, 13612–13614.
(10) Chen, G; Bare, S.R; Mallouk, T.E. Development of supported bifunctional electrocatalysts for unitized regenerative fuel cells, *J. Electrochem. Soc.* **2002**, 149, A1092–A1099.
(11) Wang, Y; Leung, D. Y.C; Xuan J; Wang, H. A review on unitized regenerative fuel cell technologies, part-A:Unitized regenerative proton exchange membrane fuel cells, *Renewable and Sustainable Energy Reviews*, **2016**, 65, 961-977.
(12) Lim, A; Lee, J. S; Lee, S; Lee, S.Y; Kim, H. J; Yoo, S. J; Jang, J. H; Sung, Y. E; Park, H. S. Polymer electrolyte membrane unitized regenerative fuel cells: Operational considerations for achieving high round trip efficiency at low catalyst loading, *Applied Catalysis B: Environmental*, **2021**, 297, 120458.
(13) Kúš, P; Ostroverkh, A; Khalakhan, I; Fiala, R; Kosto, Y; Šmíd, B; Lobko, Y; Yakovlev, Y; Nováková, J; Matolínová, I. Magnetron sputtered thin-film vertically segmented Pt-Ir catalyst supported on TiC for anode side of proton exchange membrane unitized regenerative fuel cells, *Int. J. Hydrogen Energy*, **2019**, 44, 16087-16098.
(14) Regmi, Y.N; Peng, X; Fornaciari, J.C; Wei, M; Myers, D.J; Weber, A.Z; Danilovic, N. A low temperature unitized regenerative fuel cell realizing 60% round trip efficiency and 10 000 cycles of durability for energy storage applications, *Energy Environ. Sci.*, 2020, 13, 2096-2105.
(15) Peng, X; Taie, Z; Liu, L; Zhang, Y; Peng, X; Regmi, Y. N. Fornaciari, J. C; Capuano, C; Binny, D; Kariuki, N. N; Myers, D. J; Scott, M. C; Weber, A. Z; Danilovic, N. Hierarchical electrode design of highly efficient and stable unitized regenerative fuel cells (URFCs) for long-term energy storage, *Energy Environ. Sci.* **2020**, 13, 4872-4881.
(16) Ota, K; Mitsushima, S. O_2 reduction on the Pt/polymerelectrolyte interface, *Hand. Fuel Cells*, 2010.
(17) Blizanac, B.B; Ross, P.N; Markovic, N.M. Oxygen electroreduction on Ag(1 1 1): The pH effect, *Electrochim. Acta* **2007**, 52 2264–2271.

(18) Bockris, J.M; Penner, S.S; Selman, J.R; Shores, D; Yeager, E.B; Appleby, J. Members and ex officio members of the DOE advanced fuel cell working group (AFCWG), *S.S. Penner (Ed.), Assessment of Research Needs for Advanced Fuel Cells, Pergamon*, **1986**, pp. vii–viii.
(19) Appleby A.J. Electrocatalysis. In: Conway B.E., Bockris J.O., Yeager E., Khan S.U.M., White R.E. (eds) Comprehensive Treatise of Electrochemistry, **1983**, Springer, Boston, MA.
(20) Setzler, B.P; Zhuang, Z; Wittkop, J.A. Yan, Y. Activity targets for nanostructured platinum-group-metal-free catalysts in hydroxide exchange membrane fuel cells, *Nat. Nanotechnol.* **2016**, 11, 1020–1025.
(21) Mustain, W.E; Chatenet, M; Page, M; Kim, Y.S. Durability challenges of anion exchange membrane fuel cells, *Energy Environ. Sci.* **2020**, 13, 2805 – 2838.
(22) Huang, G; Mandal, M; Peng, X; Yang-Neyerlin, A.C; Pivovar, B. S; Mustain, W.E; Kohl, P.A. *J. Electrochem. Soc.* **2019**, 166 F637.
(23) Hassan, N. U; Mandal, M; Huang, G; Firouzjaie, H. A; Kohl, P. A; Mustain, W. E. *Adv. Energy Mater.* **2020**, 10, 2001986.
(24) Mandal, M; Huang, G; Hassan, N.U; Peng, X; Gu, T; Brooks-Starks, A.H; Bahar, B; Mustain, W.E; Kohl, P.A. *J. Electrochem. Soc.* **2020**, 167 054501.
(25) Peng, X; Kulkarni, D; Huang, Y; Omasta, T. J; Ng, B; Zheng, Y; Wang, L; LaManna, J. M; Hussey, D. S; Varcoe, J. R; Zenyuk, I. V; Mustain, W. E. *Nat. Commun.* **2020**, 11, 3561.
(26) Mandal, M; Huang, G; Hassan, N. U; Mustain, W. E; Kohl, P.A. Poly (norbornene) anion conductive membranes: homopolymer, block copolymer and random copolymer properties and performance, *J. Mater. Chem. A*, **2020**, 34, 17568.
(27) Li, D; Park, E. J; Zhu, W; Shi, Q; Zhou, Y; Tian, H; Lin, Y; Serov, A; Zulevi, B; Baca, E. D; Fujimoto, C; Chung, H. T; Kim, Y. S. Highly quaternized polystyrene ionomers for high performance anion exchange membrane water electrolysers, *Nat. Energy* **2020**, 5, 378.
(28) Xiao, J; Oliveira, A. M; Wang, L; Zhao, Y; Wang, T; Wang, J; Setzler, B. P; Yan, Y. Water-Fed Hydroxide Exchange Membrane Electrolyzer Enabled by a Fluoride-Incorporated Nickel–Iron Oxyhydroxide Oxygen Evolution Electrode, *ACS Catal.* **2021**, 11, 264.
(29) Zu, Q; Oener, S. Z; Lindquist, G; Jiang, H; Li, C; Boettcher, S. W. Integrated Reference Electrodes in Anion-Exchange-Membrane Electrolyzers: Impact of Stainless-Steel Gas-Diffusion Layers and Internal Mechanical Pressure, *ACS Energy Lett*. **2021**, 6, 305.
(30) Huang, G; Mandal, M; Hassan, N. H; Groenhout, K; Dobbs, A; Mustain, W.E; Kohl, P.A. Ionomer Optimization for Water Uptake and Swelling in Anion Exchange Membrane Electrolyzer: Oxygen Evolution Electrode, *J. Electrochem. Soc*. **2021**, 167, 164514.
(31) Huang, G; Mandal, M; Hassan, N. H; Groenhout, K; Dobbs, A; Mustain, W.E; Kohl, P.A. Ionomer Optimization for Water Uptake and Swelling in Anion Exchange Membrane Electrolyzer: Hydrogen Evolution Electrode, *J. Electrochem. Soc.* **2020**, 168, 024503.
(32) Wu, X; Scott, K. A non-precious metal bifunctional oxygen electrode for alkaline anion exchange membrane cells. *J Power Sources*, **2012**, 206, 14–9.

(33) Takeguchi, T; Yamanaka, T; Takahashi, H; Watanabe, H; Kuroki, T; Nakanishi, H. Layered perovskite oxide: a reversible air electrode for oxygen evolution/reduction in rechargeable metal-air batteries, *J Am Chem Soc*. **2013**, 135, 11125–30.

(34) Ng, J. W. D; Tang, M; Jaramillo, T. F. A carbon-free, precious-metal-free, high performance O_2 electrode for regenerative fuel cells and metal-air batteries, *Energy Environ Sci*. **2014**, 7, 2017–24.

(35) Wu, X; Scott, K; Xie, F; Alford, N. A reversible water electrolyser with porous PTFE based OH− conductive membrane as energy storage cells, *J Power Sources*, **2014**, 246, 225–31.

(36) Maiyalagan, T; Jarvis, K.A; Therese, S; Ferreira, P.J; Manthiram, A. Spinel-type lithium cobalt oxide as a bifunctional electrocatalyst for the oxygen evolution and oxygen reduction reactions. *Nat Commun* **2014**, 5.

(37) Menezes, P.W; Indra, A; Sahraie, N.R; Bergmann, A; Strasser, P; Driess, M. Cobalt–manganese-based spinels as multifunctional materials that unify catalytic water oxidation and oxygen reduction reactions, *ChemSusChem* **2015**, 8, 164–71.

(38) Menezes, P.W; Indra, A; González-Flores, D; Sahraie, N.R; Zaharieva, I; Schwarze, M. High-performance oxygen redox catalysis with multifunctional cobalt oxide nanochains: morphology-dependent activity, *ACS Catal*. **2015**, 5, 2017–27.

(39) Bretthauer, C; Müller, C; Reinecke, H. A precious-metal free micro fuel cell accumulator, *J Power Sources*, **2011**, 196, 4729–34.

(40) Gayan, P; Saha, S; Liu, X; Sharma, K; Ramani, V. K. High-performance AEM unitized regenerative fuel cell using Pt-pyrochlore as bifunctional oxygen electrocatalyst, *Proceedings of the National Academy of Sciences of the United States of America*, **2021**, 118, 2107205118.

(41) Yang, F; Green, Z; Strasser, D; Shi, W; Rojas-Carbonell, S; Yan, Y; Xu, H. High-Efficiency Reversible Hydroxide Exchange Membrane Fuel Cells, *ECS Meeting Abstr*. MA, 2020-02 2439.

(42) Takasu, Y; Yoshinaga, N; Sugimoto, W. Oxygen reduction behavior of RuO2/Ti, IrO2/Ti and IrM (M: Ru, Mo, W, V) Ox/Ti binary oxide electrodes in a sulfuric acid solution, *Electrochem. Commun*. **2008**, 10, 668–672.

(43) Ge, X; Sumboja, A; Wuu, D; An, T; Li, B; Goh, F.W.T. Oxygen reduction in alkaline media: from mechanisms to recent advances of catalysts, *ACS Catal*. **2015**, 5, 4643–4667.

(44) Yang, F; Green, Z; Strasser, D; Shi, W; Rojas-Carbonell, S; Yan, Y; Xu, H. High-Efficiency Reversible Hydroxide Exchange Membrane Fuel Cells, *ECS Meeting Abstr*. MA, 2020-02 2439.

(45) Chen, G; Delafuente, D.A; Sarangapani, S; Mallouk, T.E. Combinatorial discovery of bifunctional oxygen reduction—water oxidation electrocatalysts for regenerative fuel cells, *Catal. Today*, **2001**, 67, 341–355.

(46) Yim, S.D; Park, G. G; Sohn, Y. J; Lee, W. Y; Yoon, Y. G; Yang, T. H. Optimization of PtIr electrocatalyst for PEM URFC, *Int. J. Hydrogen Energy*, **2005**, 30, 1345–1350.

(47) Yim, S. D; Lee, W. Y; Yoon, Y. G; Sohn, Y. J; Park, G. G; Yang, T. H. Optimization of bifunctional electrocatalyst for PEM unitized regenerative fuel cell, *Electrochim. Acta.* **2004**, 50, 713–718.

(48) Rivas, S; Arriaga, L.G; Morales, L; Fernandez, A.M. Evaluation of Pt-Ru-Ir as bifunctional electrocatalysts for the oxygen electrode in a unitized regenerative fuel cell, *Int. J. Electrochem. Sci.* **2012**. 7, 3601–3609.

(49) Takasu, Y; Yoshinaga, N; Sugimoto, W. Oxygen reduction behavior of RuO2/Ti, IrO2/Ti and IrM (M: Ru, Mo, W, V) Ox/Ti binary oxide electrodes in a sulfuric acid solution, *Electrochem. Commun*. **2008**, 10, 668–672.

(50) Koshikawa, H; Murase, H; Hayashi, T; Nakajima, K; Mashiko, H; Shiraishi, S; Tsuji, Y. Single nanometer-sized NiFe-layered double hydroxides as anode catalyst in anion exchange membrane water electrolysis cell with energy conversion efficiency of 74.7% at 1.0 A/cm2, *ACS Catal.* **2020**, 10, 1886–1893.

(51) Grigoriev, S.A; Pushkarev, A.S; Pushkareva, I.V; Millet, P; Belov, A.S; Novikov, V. V; Belaya, I.G; Voloshin, Y.Z. Hydrogen production by proton exchange membrane water electrolysis using cobalt and iron hexachloroclathrochelates as efficient hydrogen-evolving electrocatalysts, *Int. J. Hydrog. Energy,* **2017**, 42, 27845–27850.

(52) Li, C; Baek, J. B. The promise of hydrogen production from alkaline anion exchange membrane electrolyzers, *Nano Energy*, **2021**, 87, 106162.

(53) Mçller, S; Barwe, S; Masa, J; Wintrich, D; Seisel, S; Baltruschat, H; Schuhmann, W. Online Monitoring of Electrochemical Carbon Corrosion in Alkaline Electrolytes by Differential Electrochemical Mass Spectrometry, *Angew. Chem. Int. Ed*. **2020**, 59, 1585 – 1589.

(54) Ng, J.W; Gorlin, Y; Hatsukade, T; Jaramillo, T.F. A precious-metal-free regenerative fuel cell for storing renewable electricity, *Adv Energy Mater* **2013**, 3, 1545–50.

(55) Kormányos, A.; Speck, F. D.; Mayrhofer, K. J. J.; Cherevko, S. Influence of Fuels and PH on the Dissolution Stability of Bifunctional PtRu/C Alloy Electrocatalysts. *ACS Catal*. **2020**, 10 (19), 10858–10870.

(56) Hersbach, T. J. P.; Garcia, A. C.; Kroll, T.; Sokaras, D.; Koper, M. T. M.; Garcia-Esparza, A. T. Base-Accelerated Degradation of Nanosized Platinum Electrocatalysts. ACS Catal. 2021, 11 (15), 9904–9915.

(57) Lafforgue, C.; Zadick, A.; Dubau, L.; Maillard, F.; Chatenet, M. Selected Review of the Degradation of Pt and Pd-Based Carbon-Supported Electrocatalysts for Alkaline Fuel Cells: Towards Mechanisms of Degradation. Fuel Cells 2018, 18 (3), 229–238.

(58) Bender G; Carmo M; Smolinka T; Gago A; Danilovic N; Mueller M; Ganci F; Fallisch A; Lettenmeier P; Friedrich KA; Ayers K, Initial approaches in benchmarking and round robin testing for proton exchange membrane water electrolyzers, *International journal of hydrogen energy*. **2019**, 44, 9174-87.

(59) Young, J.L.; Kang, Z.; Ganci, F.; Madachy, S. and Bender, G., PEM electrolyzer characterization with carbon-based hardware and material sets, *Electrochemistry Communications*, 2**021**, 124, 106941.

(60) Hongsen W.; Yao Y.; Francis J. D. and Héctor D. Abruña, Multifunctional Electrocatalysts: Ru−M (M = Co, Ni, Fe) for Alkaline Fuel Cells and Electrolyzers, *ACS Catal*., **2020**,10, 8, 4608–4616.

(61) Victor S.; Melina Z.; Meital S.; David Z. and Marian Chatenet, Carbon-Supported PtNi Nanocrystals for Alkaline Oxygen Reduction and Evolution Reactions: Electrochemical Activity and Durability upon Accelerated Stress Tests, *ACS Appl. Energy Mater*. **2020**, 3, 9, 8858–8870.

(62) Lihua Z.; Qun F.; Kai L.; Sheng Z. and Xinbin Ma, First-row transition metal oxide oxygen evolution electrocatalysts: regulation strategies and mechanistic understandings, *Sustainable Energy & Fuels*, **2020**, 4, 5417-5432.
(63) Mengjie C.; Lei W.; Haipeng Y.; Shuai Z.; Hui X. and Gang W., Nanocarbon/oxide composite catalysts for bifunctional oxygen reduction and evolution in reversible alkaline fuel cells: A mini review, *J. Power Sources*, **2018**, 375, 277-290.
(64) Shiva G.; William K.;,Hui X.; Xien L.; Jaephil C. and Gang W., Bifunctional Perovskite Oxide Catalysts for Oxygen Reduction and Evolution in Alkaline Media, *Chem.AsianJ*. **2016**,11,10–21.
(65) Adabi H, Shakouri A., Hassan N. U., Varcoe J.R., Zulevi B., Serov A., Regalbuto J.R., and Mustain W.E., "High-performing commercial Fe–N–C cathode electrocatalyst for anion-exchange membrane fuel cells", *Nature Energy*, **2021**, 6, 834-843.
(66) Adabi H., Santori P.G., Shakouri A., Peng X., Yassin K., Rasin I.G., Brandon S., Dekel D.R., Hassan N. U., Sougrati M. T, Zitolo A., Varcoe J.R., Regalbuto J.R., Jaouen F. and Mustain W.E., "Understanding how Single-Atom Site Density Drives the Performance and Durability of PGM-Free Fe-N-C Cathodes in Anion Exchange Membrane Fuel Cells", *Materials Today Advances*, **2021**, 12, 100179.
(67) Jung H., Park S. and Popov B. N., Electrochemical studies of an unsupported PtIr electrocatalyst as a bifunctional oxygen electrode in a unitized regenerative fuel cell, J. Power Sources, 2009, 191, 357–361.
(68) Wang Y, Dennis Y. C. L., Xuan J., Wang H, A review on unitized regenerative fuel cell technologies, part-A: Unitized regenerative proton exchange membrane fuel cells, *Renewable and Sustainable Energy Reviews*, **2016**, 65, 961–977.
(69) Chen G, Zhang H, Ma H, Zhong H, Effect of fabrication methods of bifunctional catalyst layers on unitized regenerative fuel cell performance, *Electrochim Acta*, **2009**, 54, 5454–62.